Analytical studies on 3D hairy rotating black hole interiors

Ling-Long Gao a,b1, Yan Liua,b2 and Rui-Long Zhao a

^aCenter for Gravitational Physics, Department of Space Science, Beihang University, Beijing 100191, China

^bPeng Huanwu Collaborative Center for Research and Education, Beihang University, Beijing 100191, China

Abstract

We present an analytical study of the interior structure of hairy rotating black holes in three-dimensional Einstein gravity, minimally coupled to a complex scalar field with a sup-exponential potential. The interior dynamics of these black holes are characterized by an infinite sequence of Kasner epochs, separated by inversion and transitions, each of which admits an analytical description. We derive an explicit analytical expression for this infinite sequence of epochs. At late interior times, the geometry evolves into a curvature singularity, despite the local resemblance of each Kasner epoch to a regular Milne universe on a circle. These results reveal an interior structure richer and more complex than that of its 4D static black hole counterparts.

¹Email: linglonggao@buaa.edu.cn

²Email: yanliu@buaa.edu.cn

Contents

1	Introduction	1
2	Setup of the model	3
3	Kasner inversion and transitions	4
	3.1 Analytical description of Kasner inversion	6
	3.2 Analytical description of Kasner transitions	9
4	Analytical description of the late-time interior	13
	4.1 Behavior of the late-time singularity	20
	4.2 Comment on additional cases	23
5	Discussion	24
Α	Details of some expressions	25

1 Introduction

Three-dimensional black holes provide a mathematically tractable framework for exploring fundamental questions in quantum gravity. In three dimensions, pure Einstein gravity is topological and propagates no local dynamical degrees of freedom. Nevertheless, the BTZ black hole [1] retains key features of higher-dimensional black holes, such as an event horizon, Hawking temperature and Bekenstein-Hawking entropy. This unique combination makes BTZ black hole an ideal testing ground for the AdS/CFT correspondence (see e.g. [2–4]).

When additional matter fields are included, three-dimensional gravity supports a wider range of black hole solutions. These solutions, unlike the vacuum BTZ case, possess local dynamical degrees of freedom and typically develop curvature singularities in their interiors. Understanding these interior structures are believed to be crucial for advancing holography, though the precise holographic interpretation of the region behind the horizon remains elusive.

In higher dimensions, the interiors of static AdS–Schwarzschild black holes are described by a single Kasner geometry with fixed exponents. Various deformations to this model can alter these exponents [5]. Consequently, black hole interiors, ranging from

static to stationary configurations, have been extensively studied (see e.g. [7–23]). These developments are the AdS generalizations of the BKL dynamics. Achieving a fully analytical description of such interiors remains a central open challenge, one that is essential for constructing a complete holographic dictionary that includes the interior spacetime of black holes.

In this paper, we study asymptotically-AdS black holes in three-dimensional Einstein gravity, minimally coupled to a complex scalar field with a super-exponential potential. Our focus is on the internal structure of these hairy rotating black hole solutions. This work is directly inspired by recent studies, notably [7] and [8]. In [7], the internal structure of black holes in 3D gravity coupled to a scalar field with a potential $V = m^2 \varphi^* \varphi$ was investigated. It was shown that the geometry transitions directly from the horizon to a Kasner singularity, either with or without an inversion. Interestingly, a relation emerges among the metric field N at the boundary, horizon, and singularity, which parametrizes the off-diagonal time-angular component. In [8], planar black hole solutions in 4D gravity coupled to a scalar field with an even super-exponential potential were examined, revealing an infinite sequence of Kasner epochs. This inspired us to extend the study to 3D gravity coupled to scalar field with super-exponential potential.

The paper is organized as follows. In Sec. 2, we introduce our theoretical setup. In Sec. 3, we first choose a particular potential and present its numerical solution for black hole interiors. These solutions exhibit two different typical behaviors for the scalar field 'velocity' v (defined in (3.2)), as shown in Fig. 1 and Fig. 2. The spacetime evolves from horizon through an infinite sequence of Kasner epochs, either with or without a Kasner inversion. We then derive analytical expressions (Eqs. (3.28) and (3.29)) describing the bounce between two neighboring epochs. Unlike its 4D counterpart, where neglecting some terms during the bounce leads to monotonically decreasing |v|, the 3D dynamics allows |v| between two neighboring epochs to either decrease or increase monotonically, even inside non-rotating black holes in principle. Inside rotating black holes |v| between two neighboring epochs always increases at late times, although |v| could decrease at earlier times if an inversion occurs. It turns out that different behaviors of v are linked to the nature of the final singularity.

In Sec. 4, we derive three recurrence relations (Eqs. (4.2), (4.3) and (4.14)), from which the late-time interior evolution can be analytically solved by approximately treating the index number n of Kasner epoch as a continuous parameter. At extremely late interior times, the geometry evolves towards a special Kasner singularity with $p_t = 1$ and $p_x = 0$. It seems that such a Kasner metric describes a regular spacetime, however, the way that the interior approaches the Kasner metric indicates that it remains a curvature singularity. If an inversion occurs at a certain finite interior time, the interior could evolve towards $p_t = 0$ and $p_x = 1$ before the inversion, provided that the number of Kasner transitions

is sufficiently large. This metric describes a causal singularity in non-rotating BTZ black holes, however, the interior is again proven to remain a curvature singularity.

2 Setup of the model

We consider three dimensional gravity coupled to a complex scalar field with the following action

$$S = \int d^3x \sqrt{-g} \left(R - \partial_a \varphi \partial^a \varphi^* - V(\varphi, \varphi^*) \right) . \tag{2.1}$$

We have set $16\pi G = 1$ and the AdS radius L = 1 for convenience. The cosmological constant is included in the potential. The corresponding equations of motion are

$$R_{ab} - \frac{1}{2}Rg_{ab} = \frac{1}{2} \left(\partial_a \varphi \partial_b \varphi^* + \partial_a \varphi^* \partial_b \varphi - g_{ab} \left(\partial_c \varphi \partial^c \varphi^* + V \right) \right),$$

$$\nabla_a \nabla^a \varphi = \frac{\mathrm{d}V}{\mathrm{d}\varphi^*}.$$
(2.2)

The ansatz of hairy rotating black hole is given by³

$$ds^{2} = \frac{1}{z^{2}} \left(-fe^{-\chi} dt^{2} + \frac{dz^{2}}{f} + (Ndt + dx)^{2} \right), \quad \varphi = \phi(z)e^{-i\omega t + ikx}.$$
 (2.3)

Here f, χ, N, ϕ are functions of z. The AdS boundary is located at $z \to 0$. The horizon $z = z_H$ is determined by $f(z_H) = 0$. When we further increase the interior time $z > z_H$, the spacetime evolves toward the singularity.

Substituting the ansatz (2.3) into (2.2), we obtain the equations of motion

$$z^{3}e^{\chi/2} \left(\frac{fe^{-\chi/2}\phi'}{z} \right)' = \phi \left(k^{2}z^{2} - \frac{e^{\chi}}{f}z^{2}(\omega + kN)^{2} \right) + \frac{1}{2} \frac{dV}{d\phi},$$

$$ze^{-\chi/2} \left(\frac{e^{\chi/2}N'}{z} \right)' = \frac{2k\phi^{2}}{f}(\omega + kN),$$

$$\frac{\chi'}{2z} = \phi'^{2} + \frac{e^{\chi}\phi^{2}}{f^{2}}(\omega + kN)^{2},$$

$$2e^{\chi/2}z^{3} \left(\frac{e^{-\chi/2}f}{z^{2}} \right)' = 2k^{2}z^{2}\phi^{2} + z^{2}e^{\chi}N'^{2} + 2V.$$
(2.4)

Here primes denote derivatives with respect to z.

³Note that the wave-number n on the phase of φ was used in [7]. Here we use k instead.

3 Kasner inversion and transitions

The internal structure of black holes with a scalar potential $V=m^2\varphi^*\varphi$ was studied in [7], revealing both the disappearance of the inner horizon and the occurrence of a Kasner inversion. Separately, [8] investigated planar black hole solutions in 4D gravity coupled to a scalar field with an even super-exponential potential, reporting the presence of infinitely many Kasner transitions. Here we extend this line of inquiry by studying rotating black holes in 3D gravity, minimally coupled to a complex scalar field with a super-exponential V.

One typical scalar potential is chosen to be

$$V(\varphi, \varphi^*) = -\frac{21}{10} - \frac{3}{4} \varphi \varphi^* + \frac{1}{10} e^{\frac{1}{10}(\varphi \varphi^*)^2}. \tag{3.1}$$

At late time the interior will evolve into Kasner singularities, of which a single Kasner regime has the constant 'velocity',

$$v \equiv \frac{\mathrm{d}\phi}{\mathrm{d}\rho}\,,\tag{3.2}$$

where the coordinate ρ is introduced via

$$\rho \equiv \log z \,. \tag{3.3}$$

At the AdS boundary $\rho \to -\infty$ and at the singularity $\rho \to +\infty$. The metric functions read

$$f \sim -f_K z^{2+v^2}$$
, $\chi \sim 2v^2 \log z + \chi_1$, $N \sim N_K + \frac{E_K}{2-v^2} z^{2-v^2}$, (3.4)

where f_K, χ_1, N_K, E_K are constants. Performing the coordinate transformation

$$\tau = \frac{2}{\sqrt{f_K}(v^2 + 2)} z^{-(v^2 + 2)/2}, \qquad (3.5)$$

the metric and scalar field take the Kasner form

$$ds^{2} = -d\tau^{2} + c_{t}\tau^{2p_{t}}dt^{2} + c_{x}\tau^{2p_{x}}(N_{K}dt + dx)^{2},$$

$$\phi = p_{\phi}\log\tau + c_{\phi},$$
(3.6)

where the Kasner exponents

$$p_t = \frac{v^2}{v^2 + 2}, \quad p_x = \frac{2}{v^2 + 2}, \quad p_\phi = -\frac{2v}{v^2 + 2},$$
 (3.7)

and

$$c_t = f_K e^{-\chi_1} \left(\frac{\sqrt{f_K}(v^2 + 2)}{2} \right)^{2p_t}, \ c_x = \left(\frac{\sqrt{f_K}(v^2 + 2)}{2} \right)^{2p_x}, \ c_\phi = p_\phi \log \left(\frac{\sqrt{f_K}(v^2 + 2)}{2} \right).$$
 (3.8)

Since all Kasner exponents are expressed in terms of v, we mainly focus on the behavior of v throughout the discussion.

The following figures show the two types of the interior we have found, in addition to the disappearance of inner horizon previously found in [7] for a mass-term potential. In the left panel of Fig. 1 there are two different behaviors of the BKL singularities. On the left there are some 'decreasing' transitions where |v| between two neighboring epochs decreases toward the deeper interior, and a Kasner inversion occurs. Then the interior evolves into infinitely many 'increasing' transitions where |v| between two neighboring epochs increases as ρ increases. The right panel in Fig. 1 focuses on the Kasner inversion region. While in Fig. 2 there is no Kasner inversion and only 'increasing' transitions exist. These behaviors are different from the one in [8] where |v| between two neighboring epochs monotonically decreases as ρ increases. Note that the proper time from the first Kasner epoch to the singularity is extremely small, although the interior time coordinate ρ ranges from ρ_i to ∞ .

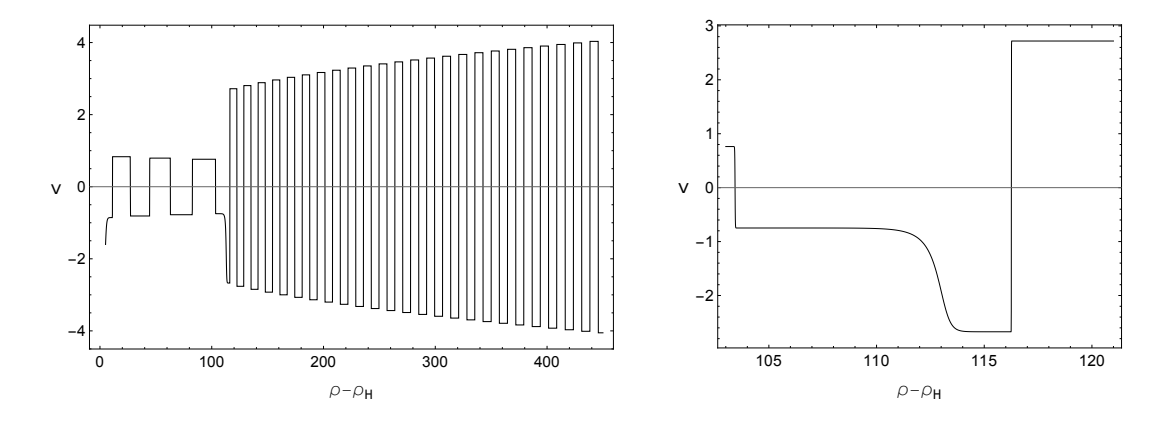


Figure 1: Evolution of v as a function of ρ . A specific set of initial values is chosen at the horizon. We name the type of left transitions as 'decreasing' transitions since |v| between two neighboring epochs decreases constantly, and the type of right ones as 'increasing' transitions. The inversion separates the two types of transitions. The right plot shows a zoomed-in view of the Kasner inversion region from the left plot.

In the following subsections we aim to derive the analytical descriptions of the Kasner inversion and transitions. After the analytical calculation we make some comments on the interior of 4D static black hole couterpart.

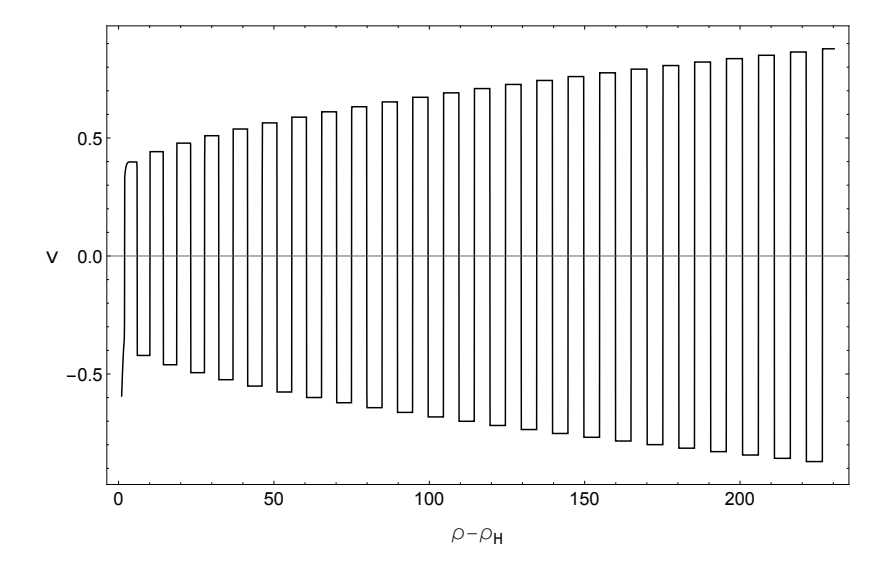


Figure 2: Evolution of v for another different choice of initial values at the horizon. There is no inversion, and only 'increasing' transitions exist in the interior.

3.1 Analytical description of Kasner inversion

The Kasner inversion is triggered by the instability of some rotation terms, such as $z^2e^{\chi}N'^2$ in (2.4), while the transitions are triggered by the potential terms, such as $\mathrm{d}V/\mathrm{d}\phi$. It can be seen from Fig. 1 that the Kasner inversion and transitions are independent of each other. That means the region where the rotation terms become unstable, does not overlap with the region where the potential terms become unstable. Therefore, in the vicinity of the Kasner inversion, all potential terms can be neglected and the equations of motion (2.4) are simplified to

$$ze^{\chi/2} \left(\frac{fe^{-\chi/2}\phi'}{z} \right)' = 0,$$

$$ze^{-\chi/2} \left(\frac{e^{\chi/2}N'}{z} \right)' = 0,$$

$$\frac{\chi'}{2z} = \phi'^2,$$

$$2e^{\chi/2}z^3 \left(\frac{e^{-\chi/2}f}{z^2} \right)' = z^2e^{\chi}N'^2.$$
(3.9)

The above simplifications are well supported by our numerical check. Thus we derive a third-order differential equation for the scalar field ϕ ,

$$\phi''' - \frac{2\phi''^2}{\phi'} + \left(z\phi'^2 - \frac{3}{z}\right)\phi'' + \phi'^3 - \frac{3\phi'}{z^2} = 0,$$
 (3.10)

where ϕ is a function of z.

Performing the transformation $z = e^{\rho}$, the above equation becomes

$$\ddot{\phi} - \frac{2\ddot{\phi}^2}{\dot{\phi}} + (\dot{\phi}^2 - 2)\ddot{\phi} = 0, \qquad (3.11)$$

which can be rewritten in terms of v via $v = \dot{\phi}$,

$$\ddot{v} - \frac{2\dot{v}^2}{v} + (v^2 - 2)\dot{v} = 0.$$
 (3.12)

Here dots denote derivatives with respect to ρ . The solution is

$$v_I = I^{-1}(\rho - \rho_I) \tag{3.13}$$

with

$$I(x) = -\frac{c_I}{2\sqrt{c_I^2 - 8}} \tanh^{-1} \left[\frac{c_I - 2x}{\sqrt{c_I^2 - 8}} \right] + \frac{1}{4} \log |x^2 - c_I x + 2| - \frac{\log |x|}{2}, \quad (3.14)$$

where c_I and ρ_I are two constants of integration. In the parameter region we considered, the function y = I(x) is one-to-one and onto and the inverse function $I^{-1}(y)$ is well-defined. We must have $c_I^2 > 8$ in order that the analytical solution matches the numerical results. We are only concerned with the two 'plateaus' of v, v_i and v_f that correspond precisely to the two values of x at which I(x) diverges. Since the $tanh^{-1}$ term dominates the divergence in (3.14) over all the other contributions, we work with the approximate inverse function

$$I_{appr}(x) = -\frac{c_I}{2\sqrt{c_I^2 - 8}} \tanh^{-1} \left[\frac{c_I - 2x}{\sqrt{c_I^2 - 8}} \right],$$
 (3.15)

which corresponds to the approximate solution for v,

$$v_{appr}^{I} = \frac{c_{I}}{2} + \frac{1}{2}\sqrt{c_{I}^{2} - 8} \tanh \left[\frac{2\sqrt{c_{I}^{2} - 8}}{c_{I}} (\rho - \rho_{I}) \right].$$
 (3.16)

Thus we have

$$v_n = \lim_{\rho \to -\infty} v_{appr}^I(\rho), \quad v_{n+1} = \lim_{\rho \to +\infty} v_{appr}^I(\rho),$$
 (3.17)

and more precisely

$$v_i = \frac{1}{2} \left(c_I - \sqrt{c_I^2 - 8} \right), \quad v_f = \frac{1}{2} \left(c_I + \sqrt{c_I^2 - 8} \right), \quad \text{if } c_I > 2\sqrt{2},$$
 (3.18)

and

$$v_i = \frac{1}{2} \left(c_I + \sqrt{c_I^2 - 8} \right), \quad v_f = \frac{1}{2} \left(c_I - \sqrt{c_I^2 - 8} \right), \quad \text{if } c_I < -2\sqrt{2}.$$
 (3.19)

The above results can be rewritten in a simpler way,

$$|v_i| = \frac{1}{2} \left(|c_I| - \sqrt{c_I^2 - 8} \right), \quad |v_f| = \frac{1}{2} \left(|c_I| + \sqrt{c_I^2 - 8} \right), \quad v_i v_f > 0,$$
 (3.20)

which permits at most one Kasner inversion

$$v \to \frac{2}{v} \,. \tag{3.21}$$

The expression for N in (3.4) within a Kasner epoch indicates that the mechanism of the Kasner inversion is as follows. If $|v| < \sqrt{2}$ for a certain Kasner epoch, then N' will become progressively larger as ρ increases. Consequently, the Kasner epoch will become unstable and an inversion occurs, until |v| is raised above the critical value $|v_c^T| = \sqrt{2}$. After the inversion, N' will decrease continuously, and the stability of a Kasner epoch will no longer be affected by rotation terms.

From Fig. 3 we observe that these transitions indeed do not affect the behavior of the metric function field N, which is consistent with the argument that the inversion and transitions are independent of each other as discussed before.⁴ We also confirm the relation of N among these values: N_h , the value of N at horizon; N_K^i , the value of N before the inversion (if it exists); and N_K^f , the value of N at late time (after the inversion). If there is no inversion, $N_K^f = 1/N_h = -k/\omega$. If the inversion occurs, $N_K^f = 1/N_K^i = N_h = -\omega/k$. The relation could be a universal behavior in 3D gravity with angular momentum coupled to a scalar field.

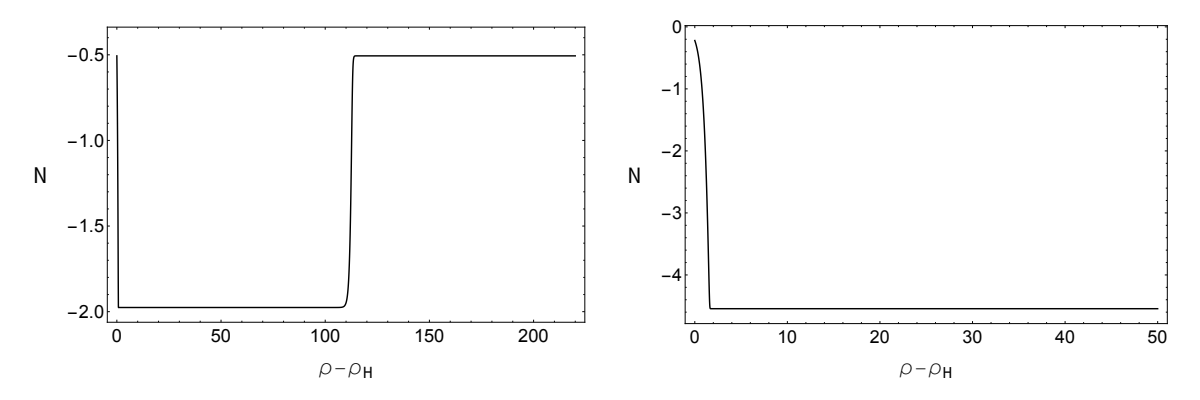


Figure 3: Evolution of N with (*left*) and without (*right*) Kasner inversion. In the left, we have $N_h = -0.506$, $N_K^i = -1.976$, and $N_K^f = -0.506$; while in the right, $N_h = -0.220$ and $N_K^f = -4.544$.

 $^{^4}$ We do not show the other extreme case of N, where there is no Kasner epoch and N is not constant before the inversion.

3.2 Analytical description of Kasner transitions

As discussed in Sec. 3.1, the Kasner inversion and transitions are independent of each other. Thus all rotation terms can be neglected and the equations of motion (2.4) are simplified to

$$z^{3}e^{\chi/2} \left(\frac{fe^{-\chi/2}\phi'}{z}\right)' = \frac{1}{2}\frac{dV}{d\phi},$$

$$\frac{\chi'}{2z} = \phi'^{2},$$

$$2e^{\chi/2}z^{3} \left(\frac{e^{-\chi/2}f}{z^{2}}\right)' = 2V.$$
(3.22)

We parameterize the potential as

$$V = e^{\int H(\phi) \, d\phi}, \qquad (3.23)$$

and derive a third-order equation for the scalar field,

$$\frac{\ddot{\phi}}{\ddot{\phi}} = \left(H + \frac{H'}{H}\right)\dot{\phi} - 2 + \left(\frac{4}{H} - 3\dot{\phi} + \frac{2\dot{\phi}^2}{H}\right)\dot{\phi} - \frac{4}{H}\ddot{\phi} + \frac{\ddot{\phi}}{\ddot{\phi}}\frac{2\dot{\phi}}{H}.$$
 (3.24)

which can be rewritten in terms of v

$$\frac{\ddot{v}}{\dot{v}} = \left(H + \frac{H'}{H}\right)v - 2 + \left(\frac{4}{H} - 3v + \frac{2v^2}{H}\right)v - \frac{4}{H}\dot{v} + \frac{\ddot{v}}{\dot{v}}\frac{2v}{H}.$$
 (3.25)

Here the prime denotes a derivative with respect to ϕ , and dots denote derivatives with respect to ρ .

It is very hard to solve the above equation directly. However, we can make an approximation within the n-th bounce

$$\left| \frac{H'}{H} \right| \ll |H| , \quad H = H_n \equiv \frac{2}{h_n} \text{ is a constant},$$
 (3.26)

which is supported by Fig. 4. Therefore, the equation (3.25) is simplified to

$$\frac{\ddot{v}}{\dot{v}} = \frac{2}{h_n}v - 2 + (2h_n - 3v + h_n v^2)v - 2h_n \dot{v} + h_n \frac{\ddot{v}}{\dot{v}}v.$$
(3.27)

The corresponding solution is a little complicated

$$v_T = T^{-1}(\rho - \rho_n),$$
 (3.28)

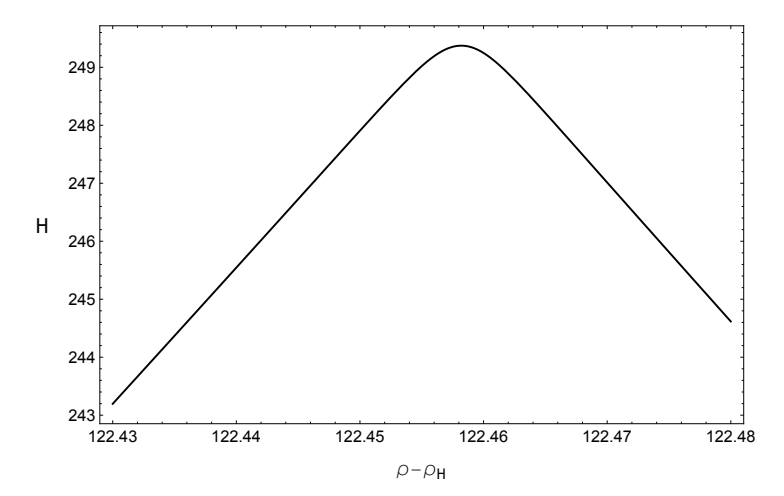


Figure 4: This figure shows that H is almost a constant H_n within a selection of an arbitrary n-th Kasner transition.

with the inverse function

$$T(x) = -\frac{c_T (1 - J_n^2)}{2J_n^2 \sqrt{c_T^2 - 4J_n^2}} \tanh^{-1} \left[\frac{c_T + 2y(x)}{\sqrt{c_T^2 - 4J_n^2}} \right] - \frac{1 - J_n^2}{2J_n^2} \log|y(x)| + \frac{1 - J_n^2}{4J_n^2} \log|y(x)|^2 + y(x)c_T + J_n^2$$
(3.29)

where

$$J_n = \sqrt{1 - 2h_n^2}, \quad y(x) = 1 - h_n x,$$
 (3.30)

and c_T and ρ_n are two constants of integration. In order that the analytical solution matches the numerical results c_T must satisfy $c_T^2 > 4J_n^2$. We are only concerned with the two 'plateaus' of $v(\rho)$, v_n and v_{n+1} that correspond to the two values of x at which T(x) diverges. Since the \tanh^{-1} term dominates the divergence over all the other contributions in (3.29), we work with the approximate inverse function

$$T_{appr}(x) = -\frac{c_T (1 - J_n^2)}{2J_n^2 \sqrt{c_T^2 - 4J_n^2}} \tanh^{-1} \left[\frac{c_T + 2y}{\sqrt{c_T^2 - 4J_n^2}} \right], \qquad (3.31)$$

which correspond to the approximate v,

$$v_{appr}^{T}(\rho) = \frac{c_T + 2}{2h_n} + \frac{\sqrt{c_T^2 - 4J_n^2}}{2h_n} \tanh \left[\frac{2J_n^2 \sqrt{c_T^2 - 4J_n^2}}{c_T (1 - J_n^2)} (\rho - \rho_n) \right].$$
 (3.32)

Thus we have

$$v_n = \lim_{\rho \to -\infty} v_{appr}^T(\rho), \quad v_{n+1} = \lim_{\rho \to +\infty} v_{appr}^T(\rho),$$
 (3.33)

and more precisely

$$v_n = \frac{c_T + 2}{2h_n} + \frac{\sqrt{c_T^2 - 4J_n^2}}{2h_n}, \quad v_{n+1} = \frac{c_T + 2}{2h_n} - \frac{\sqrt{c_T^2 - 4J_n^2}}{2h_n}, \quad \text{if } c_T < -2J_n, \quad (3.34)$$

or

$$v_n = \frac{c_T + 2}{2h_n} - \frac{\sqrt{c_T^2 - 4J_n^2}}{2h_n}, \quad v_{n+1} = \frac{c_T + 2}{2h_n} + \frac{\sqrt{c_T^2 - 4J_n^2}}{2h_n}, \quad \text{if } c_T > 2J_n.$$
 (3.35)

We could make a reasonable assumption,

$$0 < h_n < \frac{\sqrt{2}}{2} \,, \tag{3.36}$$

which is strongly supported by our numerical results that $|H| \gg 1$ within a single transition, as shown in Fig. 4. In this section we focus on the two values, $\Delta v_n = |v_{n+1}| - |v_n|$ and $s_n = v_n v_{n+1}$. The former determines whether the transitions are of increasing or decreasing type, which correspond to two absolutely different behaviors of the singularity at extremely late times, as discussed in the next section. The latter determines whether v_n alternates in sign, i.e., whether ϕ oscillates or change monotonically at late times.

Firstly, for the solution (3.34) if we begin with a Kasner epoch with $|v_n| > |v_c|$, then we have

$$c_T < -2, (3.37)$$

from which we have

$$\Delta v_n = -\frac{2 + c_T}{|h_n|} > 0, \quad s_n = -2 + \frac{2 + c_T}{h_n^2} < 0.$$
 (3.38)

Thus $|v_{n+1}| > |v_c|$ still holds and then $|v_{n+2}| > |v_{n+1}|$. Therefore, |v| always increases from bounce to bounce. This case corresponds to the 'increasing' transitions where v alternates in sign, as shown in Fig. 2 and the right portion of Fig. 1. If we begin with $|v_n| < |v_c|$, then $c_T > -2$ and there are two cases for s_n

$$\Delta v_n = -\frac{2 + c_T}{|h_n|} < 0, \quad \text{if } s_n = -2 + \frac{2 + c_T}{h_n^2} < 0,$$
 (3.39)

or

$$\Delta v_n = -\frac{\sqrt{c_T^2 - 4J_n^2}}{|h_n|} < 0, \quad \text{if } s_n = -2 + \frac{2 + c_T}{h_n^2} > 0.$$
 (3.40)

Thus $|v_{n+1}| < |v_c|$ still holds and then $|v_{n+2}| < |v_{n+1}|$. Therefore, |v| always decreases from bounce to bounce. The case (3.39) corresponds to the 'decreasing' transitions where v alternates in sign, as shown in the left portion in Fig. 1. The case (3.40) corresponds

to a step-wise decreasing $|v_n|$, however, we have not yet found this type of transitions numerically. Secondly, for the solution (3.35) $|v_n| > |v_c|$ always holds and

$$\Delta v_n = \frac{\sqrt{c_T^2 - 4J_n^2}}{|h_n|} > 0, \quad s_n = -2 + \frac{2 + c_T}{h_n^2} = \frac{1 + c_T + J_n^2}{h_n^2} > 0.$$
 (3.41)

This corresponds to a step-wise increasing $|v_n|$ that we have not found either.

In conclusion, whether |v| between two neighboring epochs increases or decreases is determined by the relative values of $|v_{in}|$, the initial value of |v|, and $|v_c| = \sqrt{2}$, the critical value that is exactly determined by the Kasner inversion. If we have $|v_{in}| < |v_c|$ for one transition, then $|v_{n+1}| < |v_n|$ holds for any value of n. While if $|v_{in}| > |v_c|$ then we have $|v_{n+1}| > |v_n|$ for any value of n. As a result, without dropping any term from (3.27), we find two types of transitions, one is 'increasing' and the other is 'decreasing'. This is consistent with our numerical results, as shown in Fig. 5.

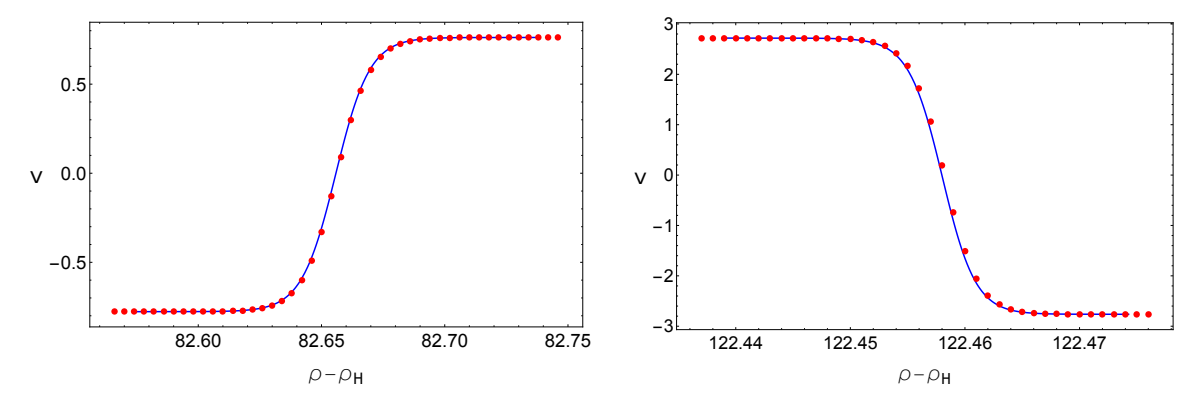


Figure 5: Evolution of v as a function of ρ within two types of Kasner transition. A bounce refers to the curve between two plateaus. The left figure shows a decreasing transition from $v_n = -0.777$ to $v_{n+1} = 0.762$, while the right shows a increasing one from $v_n = 2.719$ to $v_{n+1} = -2.763$. Solid blue lines represent the analytical results of (3.28) and (3.29). We have $\rho_n = 82.656$, $h_n = -0.0106$, $c_T = -1.99984$ for the left figure and $\rho_n = 122.458$, $h_n = 0.008$, $c_T = -2.00035$ for the right. The red points are the numerical results.

Note that the above discussion is only valid within the frame of Kasner transitions. Since we have introduced rotation, which can trigger a Kasner inversion, $|v_n|$ may be suddenly raised by (3.21) at some n. Therefore, the complete internal configuration of the BKL singularity can be described as follows: if the initial value $|v_{in}| < |v_c|$, then the interior undergoes a series of Kasner transitions, during which |v| becomes progressively smaller than $|v_c|$. Once |v| reaches a certain value $|v_0|$, the rotation terms become nonnegligible as ρ increases, leading to a Kasner inversion. As a result, |v| is raised suddenly above $|v_c|$, and no further inversion occurs, as discussed in Sec. 3.1. The interior then undergoes infinitely many transitions, with |v| between two neighboring epochs increasing

monotonically, as illustrated in Fig. 1. Similarly, if the initial value $|v_{in}| > |v_c|$, then |v| becomes progressively larger than $|v_c|$. In this case, no inversion occurs, and the interior experiences only infinitely many transitions, which is described in Fig. 2. It is important to emphasize that there are at most two types of Kasner transitions in |v| between two neighboring epochs: monotonically increasing and decreasing. This is because, under the reasonable assumption (3.36) for a super-exponential potential, the critical value for inversion exactly coincides with that for transitions. We do not focus extensively on the sign of s_n , which determines whether the scalar field oscillates or evolves monotonically at late times.

At the end of this section, we make some remarks on the interior of 4D static black hole counterpart. As discussed before, the inversion and transitions are independent processes. Therefore, within a single transition, we obtain the approximate equation (3.25) for v. This approximate equation is the same as the one in 3D non-rotating black holes, inside which we expect two types of transitions depending on the initial value of |v|. Given the structural similarity between our equation (3.25) and that in [8], we also expect these two types of transitions to exist in 4D counterpart. The only difference lies in the coefficients. By repeating the same procedure in 4D, we find that all expressions are highly similar to our results here. There the critical value of $|v_c^T| = 2\sqrt{3}$ for transitions. Furthermore, we can predict the critical value of $|v_c^I|$ for inversion (if we assume the black hole is rotating or boosting along one spatial direction) by $|v_c^I| = |v_c^T|$, which has been confirmed in [19].

The reason why only decreasing type of transitions was found in [8] is that certain terms were omitted from (3.27), resulting in a solution that only captures the decreasing transitions. This may not be problematic, as we also observe only decreasing transitions in 3D non-rotating black holes, as discussed in Sec. 4.2. However, we argue that the increasing type of transitions should not be ignored in non-rotating black holes, since it corresponds to a fundamentally different fate of the singularity at extremely late times, as discussed in the following Sec. 4.1. This remains the case even though the parameter space supporting increasing transitions constitutes a set of very small measure within the full space of solutions.

4 Analytical description of the late-time interior

To understand the late-time evolution of the interior, it is essential to derive an analytical solution for $\phi(\rho)$. Once $\phi(\rho)$ is derived, usually an approximate solution due to the extreme difficulty in obtaining an exact one, we can determine all the other metric functions using (3.22). Our strategy proceeds as follows. First, we establish three recur-

rence relations among the field velocities v_n , the field values at the bounces ϕ_n , and the locations of the bounces ρ_n , where n denotes the index number of the Kasner epoch (see Fig. 6). By treating n as a continuous variable at late times, we then solve for v(n), $\phi(n)$ and $\rho(n)$. Therefore, once the initial value of n is specified, we can determine $\phi(\rho)$ completely, and then evolve the entire spacetime. Fig. 6 illustrates the procedure for the approximate evolution of $\phi(\rho)$.

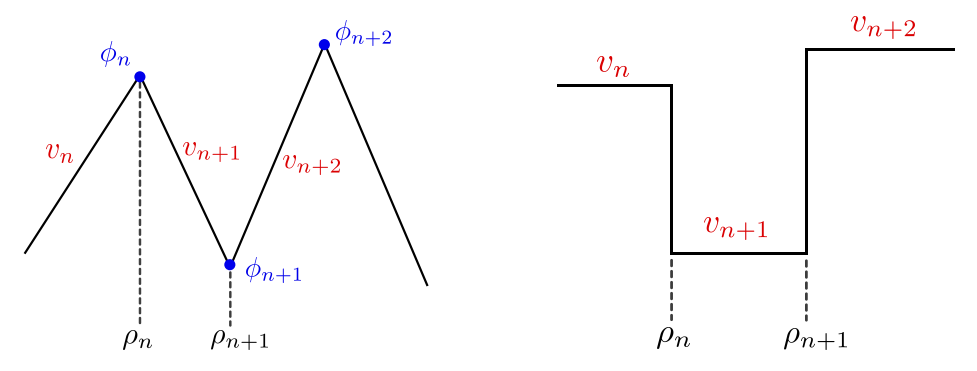


Figure 6: A schematic of the approximate evolution for $\phi(\rho)$ in ϕ - ρ plane (left) and v- ρ plane (right). Note that $\phi(\rho)$ and $v(\rho)$ are related by (3.2). In the left plot, v_n is the slop of the $\phi(\rho)$ in the n-th epoch, while in the right plot, ϕ_n is the value of ϕ at ρ_n and it satisfies (4.1). The Kasner epochs range from ρ_n to ρ_{n+1} , allowing us to set up recurrence relations for ϕ_n , v_n and ρ_n . Assuming ϕ_n , v_n and ρ_n have been obtained for arbitrary large n, then using the equation $\phi - \phi_n = v_{n+1} (\rho - \rho_n)$ we get the approximate $\phi(\rho)$ from ρ_n to ρ_{n+1} . Thus we get the full evolution of $\phi(\rho)$. The above analysis only applies when the widths of the bounces become progressively narrower than $\rho_{n+1} - \rho_n$, as we demonstrate in (4.27).

Let us first derive three recurrence relations among v_n , ϕ_n and ρ_n . Since we only find the case numerically that v and ϕ alternate in sign, we do not consider the case that v_n and v_{n+1} , ϕ_n and ϕ_{n+1} both have the same signs. That means we focus on the solution for ϕ_n where $\phi_n\phi_{n+1} < 0$, and the solution (3.34) for v_n with (3.38) and (3.39). Thus the first relation

$$\phi_{n+1} - \phi_n = v_{n+1} \left(\rho_{n+1} - \rho_n \right) \,, \tag{4.1}$$

is simplified to

$$|\phi_{n+1}| + |\phi_n| = |v_{n+1}| (\rho_{n+1} - \rho_n)$$
 (4.2)

The second relation for v_n follows from (3.34),

$$4(|v_{n+1}| - |v_n|) + 8|h_n| + |h_n|(|v_{n+1}| - |v_n|)^2 - |h_n|(|v_{n+1}| + |v_n|)^2 = 0,$$
(4.3)

which is only valid under the frame (3.38) and (3.39) we are considering. The derivation of the third relation is somewhat involved, as discussed below.

It is very useful to rewrite the equation (3.24) via (3.2) as

$$\frac{v''}{v'} = -\frac{2}{v} + \frac{H' - 2v'}{H - 2v} - \frac{v'}{v} + H - \left(v + \frac{2v'}{H - 2v}\right). \tag{4.4}$$

Note that primes denote derivatives with respect to ϕ . Integrating the above equation once we have

$$2\rho + \log \ddot{\phi} - \log V - \log (H - 2v) + \int v \,d\phi + \int \frac{2v'}{H - 2v} \,d\phi + c_l = 0, \qquad (4.5)$$

where c_l is a constant of integration. The last two terms are not integrable, however, we note from Fig. 4 that H could be regraded as a constant within a single bounce. Thus the last term could be approximately integrated to be

$$\int \frac{2v'}{H - 2v} \,d\phi \approx -\log\left(H - 2v\right). \tag{4.6}$$

Then (4.5) can be rewritten as

$$\ddot{\phi} = c_l e^{-2\rho} V (H - 2v)^2 e^{-\int v^2 d\rho} \,. \tag{4.7}$$

Using the Laplace method we get

$$v_{n+1} - v_n = \int_{\rho_n^-}^{\rho_n^+} \ddot{\phi} \, d\rho = \pm c_l \int_{\rho_n^-}^{\rho_n^+} e^{-2\rho + \log|V(H - 2v)^2| - \int v^2 \, d\rho}$$

$$\approx \pm \sqrt{2\pi c_l} e^{-\rho_n} \sqrt{V'(\phi_n)} F(\rho_n) ,$$
(4.8)

where $F(\rho)$ is defined as

$$F(\rho) \equiv e^{-\frac{1}{2} \int v^2 \,\mathrm{d}\rho} \,, \tag{4.9}$$

and we have used the following reasonable assumptions

$$\left| \frac{H'}{H} \right| \ll |H| , \quad \dot{\phi}(\rho_n) \approx 0 .$$
 (4.10)

Note that we are considering the case $v_n v_{n+1} < 0$, and thus we have

$$|v_{n+1}| + |v_n| = \sqrt{2\pi |c_l|} e^{-\rho_n} \sqrt{|V'(\phi_n)|} F(\rho_n).$$
 (4.11)

The difference $\rho_{n+1} - \rho_n$ is very useful,

$$\rho_{n+1} - \rho_n = -\log \frac{|v_{n+2}| + |v_{n+1}|}{|v_{n+1}| + |v_n|} + \log \sqrt{\left|\frac{c_l^{n+1}}{c_l^n}\right|} + \log \sqrt{\left|\frac{V'(\phi_{n+1})}{V'(\phi_n)}\right|} + \log F(\rho_{n+1}) - \log F(\rho_n).$$
(4.12)

It can be easily seen from the numerical results that the first two terms are far smaller than the other terms, and hence, (4.12) is simplified to

$$\rho_{n+1} - \rho_n = \log \sqrt{\left| \frac{V'(\phi_{n+1})}{V'(\phi_n)} \right|} - \frac{1}{2} \int_{\rho_n}^{\rho_{n+1}} v^2 \, \mathrm{d}\rho.$$
 (4.13)

The vecolity v can be regarded as a constant $v \approx v_{n+1}$ from ρ_n to ρ_{n+1} , as shown in Fig. 6. Finally we get the third recurrence relation

$$\rho_{n+1} - \rho_n = \log \sqrt{\left| \frac{V'(\phi_{n+1})}{V'(\phi_n)} \right|} - \frac{1}{2} (\rho_{n+1} - \rho_n) |v_{n+1}|^2.$$
 (4.14)

At extremely late interior times $n \to \infty$, we may consider all functions are continuous with respect to n, i.e. $|v_n| = v(n)$, $|\phi_n| = \phi(n)$, and $|\rho_n| = \rho(n)$. We can safely make the following approximations

$$|v(n+1) - v(n)| \ll \frac{4}{|h_n|}, \quad v(n+1) \approx v(n), \quad \phi(n+1) \approx \phi(n),$$
 (4.15)

and thus the three recurrence relations (4.2),(4.3) and (4.14) are simplified to

$$\frac{2\phi(n)}{v(n)} = \rho(n+1) - \rho(n),
v(n+1) - v(n) = |h(n)| (v(n)^2 - 2),
\rho(n+1) - \rho(n) = \log \sqrt{\left|\frac{V'(n+1)}{V'(n)}\right|} - \frac{1}{2} (\rho(n+1) - \rho(n)) v(n)^2.$$
(4.16)

We can use the first equation to eliminate $\rho(n)$ and get the two equations for $\phi(n)$ and v(n),

$$v(n+1) - v(n) = |h(n)| \left(v(n)^2 - 2 \right) ,$$

$$\frac{2\phi(n)}{v(n)} = \log \sqrt{\left| \frac{V'(n+1)}{V'(n)} \right|} - \phi(n)v(n) ,$$
(4.17)

which can be further transformed into two differential equations,

$$\frac{\mathrm{d}v}{\mathrm{d}n} = |h(n)| (v^2 - 2),
\frac{\mathrm{d}\phi}{\mathrm{d}n} = |h(n)| \left(\frac{2\phi}{v} + \phi v\right).$$
(4.18)

 $^{^{5}}$ It turns out the analytical solution also works well at small n, as we will show in Fig. 8.

We immediately get

$$\phi = \frac{b(2 - v^2)}{v},\tag{4.19}$$

where b is a constant of integration that depends on the types of transitions.⁶ For given values of ϕ_n and v_n , the parameter b can be determined, which yields an expression valid for arbitrary large n. In the limit of $v \to 0$,

$$\phi = \frac{2b}{v} \tag{4.20}$$

with b>0, which corresponds to the 'decreasing' transitions. And in the limit of $v\to\infty$,

$$\phi = -bv \tag{4.21}$$

with b < 0, which corresponds to the 'increasing' transitions.

Note that we have parameterized the super-exponential potential to be $V = e^{\int H d\phi}$. For the power-law $H = \lambda \phi^l$ with $\lambda, l > 0$, we have the solutions to (4.18),

$$n = n_0 + \frac{\lambda b^l (2 - v^2)^l}{4v^l (l-1)} {}_{2}F_1\left(1, \frac{1+l}{2}; \frac{3-l}{2}; \frac{v^2}{2}\right). \tag{4.22}$$

In order that the scalar field cannot escape to infinity in either direction, we restrict to even potentials, i.e., l is odd.⁷ We have

$$n - n_0 = -\frac{1}{2}\lambda b \log v \,, \quad l = 1 \,.$$

$$n - n_0 = -\frac{\lambda b^3}{4} \frac{(-4 + v^4)}{v^2} + 2\lambda b^3 \log v \,, \quad l = 3 \,.$$

$$n - n_0 = -\frac{\lambda b^5}{8} \frac{(-16 + 64v^2 - 16v^6 + v^8)}{v^4} - 12\lambda b^5 \log v \,, \quad l = 5 \,.$$

$$(4.23)$$

It can be easily seen that as $n \to \infty$, we have two different limits for $v, v \to 0$ that corresponds to the 'decreasing' transitions and $v \to \infty$ for the 'increasing' transitions. More precisely,⁸

$$n - n_0 = \frac{2^{-2+l}}{l-1} \frac{\lambda b^l}{v^{l-1}}, \quad l \in \mathbb{N}^+, l > 1, \quad \text{as} \quad v \to 0,$$
 (4.24)

and

$$n - n_0 = \frac{-\lambda b^l}{2(l-1)} v^{l-1}, \quad l \in \mathbb{N}^+, l > 1, \quad \text{as} \quad v \to \infty.$$
 (4.25)

⁶Note that after (4.18) until (4.26) in this section, ϕ , v and ρ are functions of n rather than those of z or ρ .

⁷For odd super-exponential potentials, v may evolves into a constant, since the super-exponential potential could be significantly suppressed by negative ϕ .

⁸We do not discuss the case 0 < l < 1, since it corresponds to the case that $\phi(n)$ is finite as $n \to \infty$, which could destroy the assumption that $|H(\phi_n)| \gg 1$.

For the potential (3.1), we have $\lambda = 2/5$ and l = 3. Fig. 7 and Fig. 8 show the exact agreement between (4.19), the l = 3 solution in (4.23) and our numerical results. We can also derive $\rho(v)$ by plugging (4.19) and (4.23) into the first equation in (4.16), and solve the corresponding differential equation. For l = 3 we have

$$\rho - \rho_0 = b^4 \lambda \left(\frac{4 - 12v^2 + v^6}{2v^4} - 6\log v \right). \tag{4.26}$$

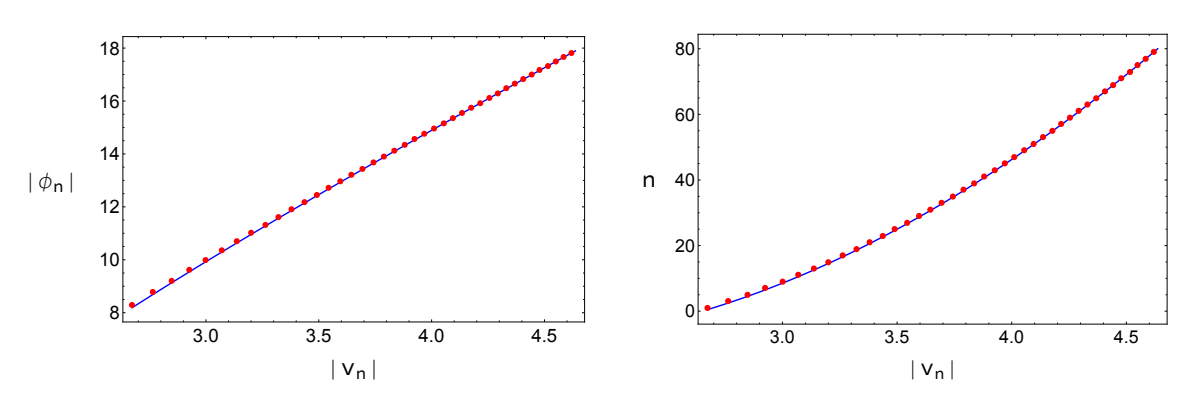


Figure 7: Behavior of $|\phi_n|$ (left) and n (right) as functions of $|v_n|$ for the increasing transitions. The red dots are numerical results, while the blue lines are analytical curves from (4.19) and (4.23) with the parameters b = -4.255, $n_0 = 10.34$.

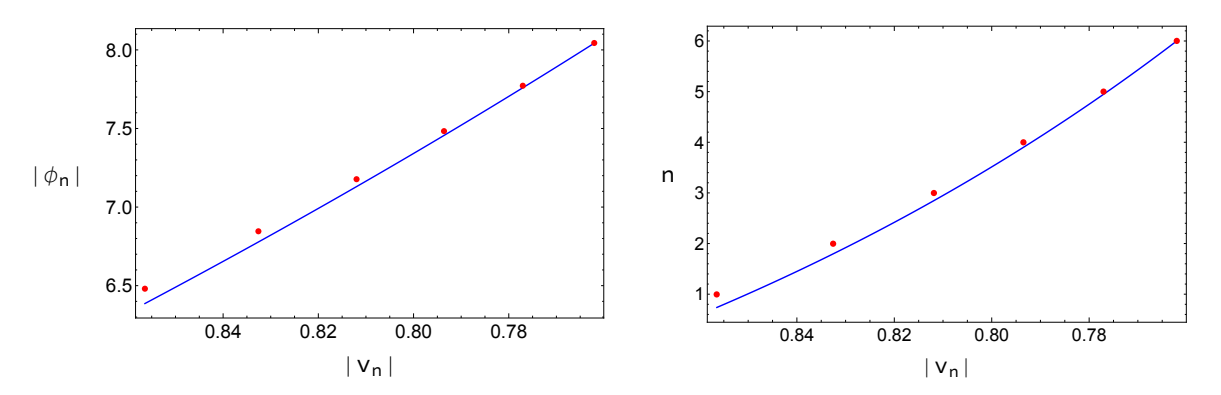


Figure 8: Behavior of $|\phi_n|$ (left) and n (right) as functions of $|v_n|$ for the decreasing transitions. The parameters b = 4.318, $n_0 = -27.29$.

Additionally, as n increases, the effective widths of bounces derived from (3.32) go to zero,

$$\left| \frac{(-1 + J_n^2)\sqrt{c_2^2 + 4J_n^2}}{2c_T J_n^2} \right| = \frac{|h_n|\sqrt{4 + (-8 + \delta v_n^2)h_n^2}}{\delta v_n (1 - 2h_n^2)} \approx \frac{2|h_n|}{\delta v_n} = \frac{4}{|H_n|\delta v_n} \approx \frac{2}{|H_n v_n|} \to 0$$
(4.27)

with $\delta v_n = |v_{n+1} - v_n| = |v_{n+1}| + |v_n|$, while the widths of Kasner epochs $|\rho_{n+1} - \rho_n|$ derived from (4.23) and (4.26) can be easily proved to be finite or divergent. Now we

have derived the expressions for ϕ_n , v_n and ρ_n , as shown in (4.19),(4.22),(4.26). Then using the relation

$$\phi - \phi_n = v_{n+1} \left(\rho - \rho_n \right) \tag{4.28}$$

we get the approximate $\phi(\rho)$ from ρ_n to ρ_{n+1} , and thus we can get the full evolution of $\phi(\rho)$ at late times.

To determine the nature of the singularity, we also need to derive the expressions for f_K^n and χ_1^n in (3.4). Note that we have obtained the approximate solution (3.32) for $v(\rho)$, plugging which into the simplified equations of motion (3.22) within a single transition we get the corresponding equations of motion for $\chi(\rho)$ and $f(\rho)$,

$$\dot{\chi} = 2(v_{appr}^T)^2,$$

$$\frac{\dot{f}}{f} = \frac{2 - 2h_n v_{appr}^T + (v_{appr}^T)^2 - h_n (v_{appr}^T)^3 + h_n \dot{v}_{appr}^T}{1 - h_n v_{appr}^T},$$
(4.29)

where dots denote derivatives with respect to ρ , namely the coordinate itself, not the function $\rho(n)$. The full solutions are lengthy and the detailed formulae can be found in Appendix A. Defining

$$f_K(\rho) \equiv -\frac{f(\rho)}{z^{2+(v_{appr}^T)^2}}, \quad \chi_1(\rho) \equiv \chi(\rho) - 2(v_{appr}^T)^2 \log z,$$
 (4.30)

within a single transition we have

$$\chi_{1}^{n} = \lim_{\rho \to -\infty} \chi_{1}(\rho), \quad \chi_{1}^{n+1} = \lim_{\rho \to +\infty} \chi_{1}(\rho),
f_{K}^{n} = \lim_{\rho \to -\infty} f_{K}(\rho), \quad f_{K}^{n+1} = \lim_{\rho \to +\infty} f_{K}(\rho).$$
(4.31)

Thus we have

$$\chi_1^{n+1} - \chi_1^n = \frac{4(c_T + 2)\rho_n \sqrt{c_T^2 - 4J_n^2}}{J_n^2 - 1} - \frac{c_T \sqrt{c_T^2 - 4J_n^2}}{J_n^2},$$

$$\log \frac{f_K^{n+1}}{f_K^n} = \frac{1}{2}(\chi_1^{n+1} - \chi_1^n) - 2\tanh^{-1} \left[-\frac{\sqrt{c_T^2 - 4J_n^2}}{c_T} \right].$$
(4.32)

Using the expression for v(n) in (3.34) to eliminate c_T and expressing J_n , h_n and ρ_n in terms of v(n), we can get $\chi_1^{n+1} - \chi_1^n$ and $\log f_K^{n+1} - \log f_K^n$ as functions of v(n). The full expressions are unnecessarily cumbersome to present here.

We shall focus on the behavior of f_K^n and χ_1^n in the limit $n \to \infty$, which corresponds to $v(n) \to \infty$ or $v(n) \to 0$. In the limit $v(n) \to \infty$ we have

$$\chi_1^{n+1} - \chi_1^n = 4bv(n)^2 - 48b\log v(n) + \left(16b - \frac{12}{b^2\lambda} + \frac{8\rho_0}{b^3\lambda}\right) + \dots,$$

$$\log \frac{f_K^{n+1}}{f_K^n} = 2bv(n)^2 - 24b\log v(n) + \left(8b - \frac{6}{b^2\lambda} + \frac{4\rho_0}{b^3\lambda}\right) + \dots.$$
(4.33)

While in the limit $v(n) \to 0$,

$$\chi_1^{n+1} - \chi_1^n = 4b + v(n)^2 \left(-8b - \frac{1}{b^2 \lambda} \right) - 12b v(n)^4 \log v(n) + \dots,$$

$$\log \frac{f_K^{n+1}}{f_K^n} = 2b + v(n)^2 \left(-4b - \frac{1}{2b^2 \lambda} \right) - 6b v(n)^4 \log v(n) + \dots.$$
(4.34)

Thus we can get the approximate differential equations for $\chi_1(n)$ and $f_K(n)$ by replacing $\chi_1^{n+1} - \chi_1^n$ with $d\chi_1/dn$, and $\log f_K^{n+1} - \log f_K^n$ with $d(\log f_K)/dn$. In the limit $v(n) \to \infty$, the leading behaviors of the solutions are

$$\chi_{1} = c_{1} - \frac{1}{2}b^{4}\lambda v^{4} + v^{2} \left(-6b^{4}\lambda + 12b^{4}\lambda \log v + 3b - 2\rho_{0} \right) - 36b \log^{2} v + 4 \log v \left(6b^{4}\lambda + \frac{3\rho_{0}}{b^{3}\lambda} - \frac{4}{b^{2}\lambda} + 8b - 1 \right) ,$$

$$\log f_{K} = c_{2} - \frac{1}{4}b^{4}\lambda v^{4} + v^{2} \left(-3b^{4}\lambda + 6b^{4}\lambda \log v + \frac{3b}{2} - \rho_{0} \right) - 18b \log^{2} v$$

$$+ 2 \log v \left(6b^{4}\lambda + \frac{3\rho_{0}}{b^{3}\lambda} - \frac{4}{b^{2}\lambda} + 8b - 2 \right) ,$$

$$(4.35)$$

where c_1 and c_2 are two constants of integration. While in the limit $v(n) \to 0$,

$$\chi_{1} = c_{3} + \frac{4b^{4}\lambda}{v^{2}} + 2\left(12b^{4}\lambda + b\right)\log v + v^{2}\left(-6b^{4}\lambda + 12b^{4}\lambda\log v - 3b - 2\rho_{0} + 1\right) + v^{4}\left(\frac{-4b^{7}\lambda^{2} + 2b^{3}\lambda + 2b + 2\rho_{0} - 1}{8b^{3}\lambda} - \frac{3}{2}b\log v\right),$$

$$\log f_{K} = c_{4} + \frac{2b^{4}\lambda}{v^{2}} + \left(12b^{4}\lambda + b\right)\log v + v^{2}\left(-3b^{4}\lambda + 6b^{4}\lambda\log v - \frac{3b}{2} - \rho_{0} + 1\right) + v^{4}\left(\frac{-2b^{7}\lambda^{2} + 2b^{3}\lambda + b + \rho_{0} - 1}{8b^{3}\lambda} - \frac{3}{4}b\log v\right),$$

$$(4.36)$$

where c_3 and c_4 are two constants of integration. We have verified that the above analytical solutions agree well with the numerical results. These solutions are useful for determining whether the interior evolves towards a curvature singularity at extremely late times.

4.1 Behavior of the late-time singularity

The late-time evolution of the interior remains the same, regardless of whether an inversion occurs, as early shown in Fig. 1 and Fig. 2. Hence, we restrict our attention to the

⁹Since we do not have sufficient data for decreasing transitions in the interior shown in Fig. 1, the subleading terms v^2 and v^4 are essential for ensuring the high accuracy of the solutions, although they will not have an effect on determining the nature of the singularity in the next subsection.

case with inversion. Note that we have verified that $N_K^f = N_h$ is always a constant after the inversion in Sec. 3.1. Performing the transformation

$$y = N_K^f t + x \,, \tag{4.37}$$

where y has the same period as x, namely 2π , within a single Kasner epoch the metric (3.6) reads

$$ds^{2} = -d\tau^{2} + c_{t}\tau^{2p_{t}}dt^{2} + c_{x}\tau^{2p_{x}}dy^{2}.$$
(4.38)

During the transitions from one Kasner epoch to the next, the field velocity v approaches infinity at extremely late-times, as indicated in (4.25). Thus, it follows from (3.7) that after the inversion, the Kasner exponents evolves towards

$$p_t \to 1$$
, $p_x \to 0$, $p_\phi \to 0$. (4.39)

Firstly, we aim to determine the spacetime described by the Kasner metric (4.38) with exactly $p_t = 1$ and $p_x = 0$. It is not the singularity in non-rotating BTZ black holes with $p_t = 0$ and $p_x = 1$, despite having the same local geometry. The metric can be deformed into

$$ds^{2} = -d\tau^{2} + \tau^{2}d\tilde{t}^{2} + c_{x}dy^{2}, \qquad (4.40)$$

which is the two dimensional Milne universe cross a circle, namely, $\operatorname{Milne}_{1+1} \times S^1$. There is no curvature singularity since all curvature invariants are finite. We can also prove that no causal singularity, which appears in non-rotating BTZ black holes, arises. Assuming a closed timelike curve $\tau(\lambda)$, $\tilde{t}(\lambda)$, $y(\lambda)$ exists, we have

$$ds^{2} = -\frac{d\tau^{2}}{d\lambda^{2}} + \tau^{2} \frac{d\tilde{t}^{2}}{d\lambda^{2}} + c_{x} \frac{dy^{2}}{d\lambda^{2}} < 0.$$
(4.41)

Since τ will come back to its value at t_0 , it has to be such that $d\tau/d\lambda = 0$ at some value of λ . Then at this point, $d\tilde{t}/d\lambda$ and $dy/d\lambda$ must also be zero so that the curve terminates at this point, and a contradiction arises. Actually, $Milne_{1+1}$ universe only covers half of 1+1 dimensional Minkowski spacetime. Even if we extend the $Milne_{1+1} \times S^1$ to the other patch of $Minkowski_{1+1} \times S^1$, which corresponds to the region $\tau^2 < 0$, there is still no closed timelike curve.

One might naively expect that this would provide another way to realize black holes with regular interiors beyond the setup in [24]. However, the following careful examination of the curvature of (4.38) with (4.39) shows it actually diverges as $\tau \to 0$. It turns out that the key mechanism determining the nature of the singularity is the non-commutativity between the $\tau \to 0$ and $p_t \to 1$ $(v \to \infty)$ limits.

The curvature of (4.38) reads

$$R = R_{\mu\nu}R^{\mu\nu} = \frac{2p_t(p_t - 1)}{\tau^2}, \quad R_2 = R_{\mu\nu\alpha\beta}R^{\mu\nu\alpha\beta} = 3R^2.$$
 (4.42)

It is sufficient to focus only on the late-time behavior of R, which can be expressed in terms of v,

$$R(\tau; v) = -\frac{4v^2}{(2+v^2)^2 \tau^2}.$$
(4.43)

If we first take the limit $v \to \infty$, followed by $\tau \to 0$, then it indeed describes a singularity evolving towards the regular spacetime Milne₁₊₁ × S^1 . But our case is far different. Within a given Kasner regime, the proper time τ is not free to approach to zero. Or equivalently the coordinate z is not free to approach infinity. Instead, it is constrained to lie in a range approximately from $e^{\rho_{n-1}}$ to e^{ρ_n} , which is supported by (4.27) that the effective widths of bounces vanish. Thus τ is constrained by (3.5) in the range (τ_{n-1}, τ_n) with

$$\tau_{n-1} = \frac{2}{\sqrt{f_K^n(v_n^2 + 2)}} e^{-\rho_{n-1}(v_n^2 + 2)/2} , \quad \tau_n = \frac{2}{\sqrt{f_K^n(v_n^2 + 2)}} e^{-\rho_n(v_n^2 + 2)/2} . \tag{4.44}$$

Note that |R| increases monotonically as τ decreases in the range. Thus we focus on the maximum of |R|,

$$R_m = |R(\tau_n, v_n)| = \frac{4v_n^2}{(2 + v_n^2)^2 \tau_n^2}.$$
(4.45)

Plugging (4.26), (4.35) and (4.44) into the above expression we have

$$\log R_m = \frac{1}{4}b^4 \lambda v^4 + v^2 \left(\frac{3b}{2} - 2b^4 \lambda\right) + \log v \left(\frac{6\rho_0}{b^3 \lambda} - \frac{8}{b^2 \lambda} + 16b - 2\right) - 18b \log^2 v + c_2 - 6b^4 \lambda + 2\rho_0 + O(\frac{1}{v^2}),$$
(4.46)

which is again in excellent agreement with our numerical data. We can clearly see that as $v \to \infty$, the curvature increases progressively from one Kasner epoch to the next, and therefore the singularity remains a curvature one at late times.

Now we consider the case in which, before the inversion, the Kanser transition occurs large number of times.¹⁰ Since the metric function N is a constant, $N_K^i = 1/N_h = -k/\omega$ as discussed in Sec. 3.1, within a single Kasner epoch the metric (3.6) can also be deformed into (4.38). We can see from (4.24) that $v \to 0$ at large n, and thus the Kasner exponents evolves towards

$$p_t \to 0$$
, $p_x \to 1$, $p_\phi \to 0$, (4.47)

which fortuitously exchanges p_t and p_x in (4.39). This is traceable. From (3.21), we find that the inversion exchanges the values of p_t and p_x before and after the inversion. Here, similarly, the inversion exchanges the evolution directions of the transitions. The same

¹⁰We do not have to fine-tune the initial values at the horizon, whereas we only need to choose the initial values carefully.

question arises: whether the interior evolves towards the non-curvature singularity with $p_t = 0$ and $p_x = 1$, which is the singularity in non-rotating BTZ black holes. The analysis here is the same as that in the case $v \to \infty$. We have

$$\log R_m = \frac{4b^4\lambda}{v^4} - \frac{8b^4\lambda}{v^2} + (b+2)\log v + c_4 - 6b^4\lambda + 2\rho_0 + O(v^2), \qquad (4.48)$$

showing equally good agreement with our numerical results. The curvature becomes progressively larger, and the singularity still remains a curvature one. It should be emphasized that the above late-time behavior may appear only when the inversion exists. If the initial $|v| > |v_c|$, no inversion occurs, and the interior only evolves towards (4.39) while the curvature diverges.

4.2 Comment on additional cases

In the previous sections, we examined the co-effect of the rotation and a complex scalar field with a super-exponential potential (3.1). However, we find that in the presence of a super-exponential potential, the simplified equations of motion in the vicinity of a single transition are independent of whether the scalar field is real or complex, and also independent of whether the black hole is rotating or not. That means we can utilize (4.19) and (4.23) to discuss the three additional cases:

- (i) N is non-trivial and $\omega = k = 0$: rotating black holes with a real scalar field,
- (ii) $N = \omega = 0$ and $k \neq 0$: non-rotating black holes with a complex scalar field, and
- (iii) $N = \omega = k = 0$: non-rotating black holes with a real scalar field.

The corresponding numerical results are shown in Fig. 9.

Firstly, the case (i) is a little different from the other two cases. Because of the presence of the rotation, an inversion could occur so that there could exist two types of transitions in the interior, which is expected to be similar to that shown in Fig. 1. However, we only find the increasing type of transitions, which is very similar to that shown in Fig. 2. This indicates an inversion could not exist for case (i), and hence, the initial value of |v|, v_0 is always greater than $|v_c|$. This is consistent with our earlier numerical results in [7], although an analytical proof is still lacking.

Secondly, for cases (ii) and (iii) there are no "unstable" rotation terms and we expect no inversion to occur. The transitions are of either decreasing or increasing type within a given black hole interior, which depends on whether $|v_0| > |v_c|$. However, we only find the increasing type of transitions in case (ii), while the decreasing type occurs in case (iii). This indicates $|v_0|$ is always greater than $|v_c|$ in case (ii), while $|v_0| < |v_c|$ always holds in case (iii). Therefore, the cases (ii) and (iii) have absolutely different late-time evolution.

Finally, we conclude this section with a question: why the initial value of |v| is not completely free, but constrained to lie either above or below the critical value $|v_c|$. From the perspective of the equations of motion, no such constraint is apparent. This discrepancy may originate from additional physical restrictions inside the black hole, which would be worth further investigation, or it might simply reflect the incompleteness of our numerical exploration of the parameter space.

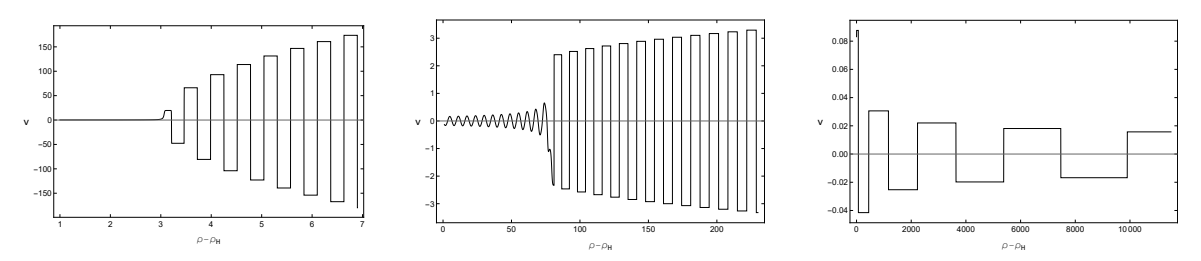


Figure 9: The evolution of v as a function of $\rho - \rho_H$ in cases (i), (ii) and (iii), from left to right. All of these numerical results are in agreement with (4.19) and (4.23).

5 Discussion

We have presented an analytical study of the interior structure of hairy, rotating black holes in 3D Einstein gravity minimally coupled to a scalar field with a sup-exponential potential. Both Kasner inversion and transitions between consecutive Kasner epochs admit analytical solutions. Moreover, we have derived an explicit analytical expression that characterize the infinite sequence of Kasner epochs deep inside the horizon.

At late interior times, despite each individual epoch locally resembling a regular Milne universe on a circle, a careful asymptotic analysis of the interplay between $v \to \infty$ and $\tau \to 0^+$ reveals that the geometry remains a curvature singularity. Thus, the final nature of this singularity is distinct from that of the rotating BTZ black hole. This contrasts with the four-dimensional, non-rotating case, where the singularity was found to be identical to that of a Schwarzschild black hole [8].

There are lots of open questions for future study. The analytical description of the Kasner sequence could play a key role in exploring the holographic dual of black hole interiors. In particular, from the perspective that spacetime geometry emerges from quantum entanglement [25], it would be highly interesting to identify the dual CFT structures responsible for each Kasner epoch and for the infinite cascade of transitions.

As we approach the singularity, the spatial volume shrinks to zero. This is the time reverse of a cosmological evolution through an infinite sequence of Kasner epochs near $\tau = 0^+$. It would be intriguing to investigate whether this interior dynamics could be

reversed to construct new, exactly solvable models of the early universe. Furthermore, the bouncing structure of Kasner epochs represents a non-chaotic evolution near the singularity. In contrast, more complicated initial conditions in the BKL picture are expected to give rise to chaotic behavior [6, 26]. Constructing a simple chaotic BKL system that can be analytically described would be an interesting challenge.

While our description assumes the validity of classical gravity, it is well known that quantum effect become important in regions of large curvature. The super-exponential potential might arise from higher dimensional reduction, which itself should be an interesting topic for further study. Realizing this reduction from a UV-complete theory, perhaps through a consistent embedding in string theory, could offer new insights into the quantum nature of the black hole interior. Additionally, exploring the quantization of interior geometry via the Wheeler–DeWitt equation [27,28] and examining singularity resolution in this context could be useful for our understanding of quantum gravity.

Acknowledgments

We thank Hong-Da Lyu, Ya-Wen Sun, You-Jie Zeng, Yu Zhou for useful discussions. This work is supported by the National Natural Science Foundation of China grant No. 12375041 and 12575046.

A Details of some expressions

In this appendix, we show details of some expressions in Sec. 4. The full solutions for $\chi(\rho)$ and $f(\rho)$ to (4.29) are

$$\chi(\rho) = c_{\chi} - \frac{2a_{2}^{2}}{a_{3}} \tanh \left[a_{3} \left(\rho - \rho_{n} \right) \right] + \frac{(a_{1} - a_{2})^{2}}{a_{3}} \log \left[\tanh \left[a_{3} \left(\rho - \rho_{n} \right) \right] + 1 \right]$$

$$- \frac{(a_{1} + a_{2})^{2}}{a_{3}} \log \left[1 - \tanh \left[a_{3} \left(\rho - \rho_{n} \right) \right] \right] ,$$

$$f(\rho) = c_{f} \frac{\cosh^{\frac{2a_{1}a_{2}}{a_{3}} + 1} \left[a_{3} \left(\rho - \rho_{n} \right) \right] e^{\left(a_{1}^{2} + a_{2}^{2} + 2 \right) \left(\rho - \rho_{n} \right) - \frac{a_{2}^{2}}{a_{3}} \tanh \left[a_{3} \left(\rho - \rho_{n} \right) \right] - \rho \left(\left(a_{1} + a_{2} \tanh \left[a_{3} \left(\rho - \rho_{n} \right) \right] \right)^{2} + 2 \right)}{a_{2}h_{n} \sinh \left[a_{3} \left(\rho - \rho_{n} \right) \right] + \left(a_{1}h_{n} - 1 \right) \cosh \left[a_{3} \left(\rho - \rho_{n} \right) \right]}$$

$$(A.1)$$

where c_{χ} and c_f are two constants of integration. From the limit defined in (4.31), we have

$$\chi_1^n = c_{\chi} - 2(a_1 + a_2)^2 \rho_n - \frac{2a_2(a_2 + 2a_1 \log 2)}{a_3},$$

$$\chi_1^{n+1} = c_{\chi} - 2(a_1 - a_2)^2 \rho_n + \frac{2a_2(a_2 - 2a_1 \log 2)}{a_3},$$
(A.2)

and

$$f_K^n = c_f \frac{4^{-\frac{a_1 a_2}{a_3}} e^{-((a_1 + a_2)^2 + 2)\rho_n - \frac{a_2^2}{a_3}}}{a_1 h_n + a_2 h_n - 1},$$

$$f_K^{n+1} = c_f \frac{4^{-\frac{a_1 a_2}{a_3}} e^{-((a_1 - a_2)^2 + 2)\rho_n + \frac{a_2^2}{a_3}}}{a_1 h_n - a_2 h_n - 1}.$$
(A.3)

Note that between two neighboring epochs during the transitions, we have rewritten the approximate solution (3.32) for v as

$$v_{appr}^{T} = a_1 + a_2 \tanh \left[a_3(\rho - \rho_n) \right],$$
 (A.4)

with

$$a_1 = \frac{2 + c_T}{2h_n}, \quad a_2 = \frac{\sqrt{c_T^2 - 4J_n^2}}{2h_n}, \quad a_3 = \frac{J_n^2 \sqrt{c_T^2 - 4J_n^2}}{c_T h_n^2}.$$
 (A.5)

From these expressions, one obtains the recurrence relations (4.32) for χ_1^n and f_K^n .

References

- [1] M. Banados, M. Henneaux, C. Teitelboim and J. Zanelli, *Geometry of the (2+1) black hole*, Phys. Rev. D **48** (1993), 1506-1525 [erratum: Phys. Rev. D **88** (2013), 069902] [arXiv:gr-qc/9302012].
- [2] W. Li, W. Song and A. Strominger, *Chiral Gravity in Three Dimensions*, JHEP **04** (2008), 082 [arXiv:0801.4566].
- [3] Y. Liu and Y. W. Sun, Note on New Massive Gravity in AdS(3), JHEP **04** (2009), 106 [arXiv:0903.0536].
- [4] A. Castro, M. R. Gaberdiel, T. Hartman, A. Maloney and R. Volpato, *The Gravity Dual of the Ising Model*, Phys. Rev. D **85** (2012), 024032 [arXiv:1111.1987].
- [5] A. Frenkel, S. A. Hartnoll, J. Kruthoff and Z. D. Shi, *Holographic flows from CFT to the Kasner universe*, JHEP **08**, 003 (2020) [arXiv:2004.01192].

- [6] V. Belinski and M. Henneaux, *The Cosmological Singularity*, Cambridge Universe Press.
- [7] L. L. Gao, Y. Liu and H. D. Lyu, Internal structure of hairy rotating black holes in three dimensions, JHEP **01** (2024), 063 [arXiv:2310.15781].
- [8] S. A. Hartnoll and N. Neogi, AdS black holes with a bouncing interior, SciPost Phys. 14, no.4, 074 (2023) [arXiv:2209.12999].
- [9] S. A. Hartnoll, G. T. Horowitz, J. Kruthoff and J. E. Santos, *Gravitational duals to the grand canonical ensemble abhor Cauchy horizons*, JHEP **10**, 102 (2020) [arXiv:2006.10056].
- [10] Y. Q. Wang, Y. Song, Q. Xiang, S. W. Wei, T. Zhu and Y. X. Liu, *Holographic flows with scalar self-interaction toward the Kasner universe*, [arXiv:2009.06277].
- [11] L. Sword and D. Vegh, What lies beyond the horizon of a holographic p-wave super-conductor, JHEP 12 (2022), 045 [arXiv:2210.01046].
- [12] Y. Liu, H. D. Lyu and A. Raju, *Black hole singularities across phase transitions*, JHEP **10**, 140 (2021) [arXiv:2108.04554].
- [13] Y. Liu and H. D. Lyu, *Interior of helical black holes*, JHEP **09**, 071 (2022) [arXiv:2205.14803].
- [14] Y. S. An, L. Li, F. G. Yang and R. Q. Yang, Interior structure and complexity growth rate of holographic superconductor from M-theory, JHEP **08**, 133 (2022) [arXiv:2205.02442].
- [15] R. G. Cai, M. N. Duan, L. Li and F. G. Yang, Towards classifying the interior dynamics of charged black holes with scalar hair, JHEP **02** (2024), 169 [arXiv:2312.11131].
- [16] X. K. Zhang, X. Zhao, Z. Y. Nie, Y. P. Hu and Y. S. An, Diving into a holographic multi-band superconductor, Phys. Lett. B 868 (2025), 139684 [arXiv:2411.07693].
- [17] D. Areán, H. S. Jeong, J. F. Pedraza and L. C. Qu, Kasner interiors from analytic hairy black holes, JHEP 11 (2024), 138 [arXiv:2407.18430].
- [18] E. Caceres, S. Shashi and H. Y. Sun, *Imprints of phase transitions on Kasner sin-gularities*, Phys. Rev. D **109** (2024) no.12, 126018 [arXiv:2305.11177].
- [19] H. L. Prihadi, R. R. Firdaus, F. Khairunnisa, D. Dwiputra and F. P. Zen, Stationary Solution to Charged Hairy Black Hole in AdS4: Kasner Interior, Rotating Shock Waves, and Fast Scrambling, [arXiv:2508.02174].
- [20] L. L. Gao, Y. Liu and H. D. Lyu, Black hole interiors in holographic topological semimetals, JHEP **03**, 034 (2023) [arXiv:2301.01468].
- [21] J. Carballo, A. K. Patra and J. F. Pedraza, Diving inside holographic metals, JHEP 05 (2025), 072 [arXiv:2408.07748].

- [22] E. Cáceres, A. J. Murcia, A. K. Patra and J. F. Pedraza, Kasner eons with matter: holographic excursions to the black hole singularity, JHEP 12 (2024), 077 [arXiv:2408.14535].
- [23] G. Oling and J. F. Pedraza, Mixmasters in Wonderland: Chaotic dynamics from Carroll limits of gravity, SciPost Phys. Core 8 (2025), 025 [arXiv:2409.05836].
- [24] P. Bueno, O. Lasso Andino, J. Moreno and G. van der Velde, *On regular charged black holes in three dimensions*, JHEP **25** (2025), 132 [arXiv:2503.02930].
- [25] J. M. Maldacena, Eternal black holes in anti-de Sitter, JHEP **04** (2003), 021 [arXiv:hep-th/0106112].
- [26] P. Fleig and V. A. Belinski, BKL oscillations in 2+1 space-time dimensions, [arXiv:1811.05208].
- [27] S. A. Hartnoll, Wheeler-DeWitt states of the AdS-Schwarzschild interior, JHEP **01** (2023), 066 [arXiv:2208.04348].
- [28] E. Cáceres and H. Krishna, On thermal holographic RG flows, [arXiv:2510.09955].